





22 **Abstract:** For computationally efficient modeling of unsaturated-saturated flow  
23 systems of regional scale, it is necessary to use Quasi three-dimensional (3-D) schemes  
24 that consider one-dimensional (1-D) soil water flow and 3-D groundwater flow.  
25 However, it is still practically challenging for regional-scale problems due to the high  
26 non-linear and intensive input data needed for soil water modeling, the reliability of the  
27 coupling scheme, and the complicated modeling operation. This study developed a new  
28 Quasi-3D model coupled the soil water balance model UBMOD with MODFLOW. A  
29 new iterative scheme was developed, in which the vertical net recharge and unsaturated  
30 zone depth were used as the exchange information. A modeling framework was  
31 developed by Python script to wrap the coupled model, the pre- and the post-process  
32 modules, which gave a comprehensive modeling tool from data preparation to results  
33 displaying. The strength and weakness of the coupled model are evaluated by using two  
34 published studies. The comparison results show that the coupled model is satisfactory  
35 in terms of computational accuracy, mass balance error and cost. Additionally, the  
36 coupled model is used to evaluate groundwater recharge in a real-world study. The  
37 measured groundwater table and soil water content are used to calibrate the model  
38 parameters, and the groundwater recharge data from a two years' tracer experiment is  
39 used to evaluate the recharge estimation. The field application further shows the  
40 practicability of the model. The developed model and the modeling framework provide  
41 a convenient and flexible tool for evaluating unsaturated-saturated flow system at the  
42 regional scale.

43

44

## 45 **1 Introduction**

46 While groundwater resource is important for the domestic, agricultural, and  
47 industrial uses, groundwater is vulnerable due to over-exploitation, climate change, and  
48 biochemical pollution (Bouwer, 2000; Sophocleous, 2005; Evans and Sadler, 2008;



49 Karandish et al., 2015; Zhang et al., 2018). For protecting or exploiting groundwater  
50 resource, understanding soil water flow system is necessary as soil water is the major  
51 source of groundwater recharge and destination of phreatic consumption (Yang et al.,  
52 2016; Wang et al., 2017). **The extended form** of the Richards' equation is usually used  
53 to describe the soil water flow and groundwater flow. Many numerical schemes have  
54 been developed to solve the three-dimensional (3-D) Richards' equation (Weill et al.,  
55 2009) in computer codes, such as HYDRUS (Šimůnek et al., 2012), FEFLOW (Diersch,  
56 2013), HydroGeoSphere (Brunner and Simmons, 2012), InHM (VanderKwaak and  
57 Loague, 2001) and MODHMS (Tian et al., 2015). Since the soil water flow is highly  
58 nonlinear in nature and sensitive to atmospheric changes, soil utilizations, and human  
59 activities, the numerical schemes require using fine discretization in space and time for  
60 accurate numerical solutions (Downer and Ogden, 2004; Varado et al., 2006). This  
61 makes the numerical solutions computationally expensive, especially for large scale  
62 modeling; the fine discretization also leads to a mismatch with saturated groundwater  
63 flow, because the latter solutions are commonly based on coarse discretization. (Van  
64 Walsum and Groenendijk, 2008; Shen and Phanikumar, 2010; Yang et al., 2016;  
65 Szymkiewicz et al., 2018).

66 To address the computational challenges discussed above, a variety of  
67 simplifications have been introduced for the soil water flow for regional scale problems.  
68 One simplification is to treat the hydrological processes (e.g., infiltration,  
69 evapotranspiration, and deep percolation) occurring in the unsaturated zone as one-



70 dimensional (1-D) processes in the vertical direction. Field experiments at the regional  
71 scale also show that, in the unsaturated zone, the lateral hydraulic gradient is usually  
72 significantly smaller than the vertical gradient (Sherlock et al., 2002). This 1-D  
73 simplification leads to the Quasi-3D scheme, which ignores the lateral flow in the  
74 unsaturated zone but considers groundwater flow as a 3-D problem. The Quasi-3D  
75 scheme avoids solving the 3-D Richards' equation for the unsaturated zone, and thus  
76 improves computational efficiency and model stability. The Quasi-3D scheme is the  
77 most efficient solution for large-scale unsaturated-saturated flow modeling (Twarakavi,  
78 et al., 2008; Yang et al., 2016) and is popular among groundwater modelers (Havard et  
79 al., 1995; Harter and Hopmans, 2004; Graham and Butts, 2005; Stoppelenburg et al.,  
80 2005; Seo et al., 2007; Markstrom et al., 2008; Ranatunga et al., 2008; Kuznetsov et al.,  
81 2012; Xu et al., 2012; Zhu et al., 2012; Maxwell et al., 2014; Leterme et al., 2015).  
82 However, it is still challenging when using the Quasi-3D models for a practical regional  
83 scale problem. Three concerns arise as follows.

84         The first concern is the unsaturated modeling method. Although the Quasi-3D  
85 scheme is computationally efficient, the numerical solutions of the 1-D Richards'  
86 equation still require intensive input data, and face numerical instability and mass  
87 balance errors under some specific situations such as infiltration into the dry soil (Zha  
88 et al., 2017), which limit their practical application to simulating regional scale  
89 problems under complicated geological and climate conditions as well as anthropogenic  
90 activities. As an alternative to the numerical solutions of the 1-D Richards' equation,



91 water balance models have been used to describe soil water movements, which not only  
92 reduces the amount of input data but also further improve computational efficiency and  
93 stability for simulating soil water movement. The water balance models can be coupled  
94 with groundwater models. Facchi et al. (2004) coupled a conceptual soil water  
95 movement model SWAT with MODFLOW to simulate the hydrological relevant  
96 processes in the alluvial irrigated plains. Kim et al. (2008) integrated SWAT with  
97 MODFLOW to describe the exchange between hydrologic response units in the SWAT  
98 model and MODFLOW cells. The traditional water balance models however, may  
99 oversimplify soil water movement, and thus cannot accurately represent certain  
100 important features of soil water flow, e.g., the upward flux and soil heterogeneity. Mao  
101 et al. (2018) developed a soil water balance model (called UBMOD model) based on  
102 the hybrid of numerical and statistical methods. In particular, UBMOD can simulate  
103 both upward and downward soil water movement in heterogeneous situation with only  
104 four model parameters, and the model can be used with a coarse discretization in space  
105 and time, all of which make it suitable for the large-scale modeling.

106 Another concern is the scheme when coupling saturated models with unsaturated  
107 models. There are three different numerical coupling schemes categorized by Furman  
108 (2008): uncoupled, iterative coupled, and fully coupled. The uncoupled scheme is  
109 widely used when using soil water flow packages with MODFLOW, such as  
110 LINKFLOW (Havard et al., 1995), SVAT-MODFLOW (Facchi et al., 2004), UZF1-  
111 MODFLOW (Niswonger et al., 2006), HYDRUS-MODFLOW (Seo et al., 2007),



112 SWAP-MODFLOW (Xu et al., 2012). While this scheme is easy to be implemented,  
113 its results may not reliable when recharge from the unsaturated zone causes substantial  
114 changes of water table. Additionally, this scheme may result in the mass balance error  
115 (Shen and Phanikumar, 2010; Kuznetsov et al., 2012). The fully coupled scheme is  
116 mathematically and computationally rigorous, because it solves unsaturated and  
117 saturated flows simultaneously with internal boundary conditions of the two flows (Zhu  
118 et al., 2012). However, the fully coupled scheme is computationally expensive (Furman,  
119 2008). The iterative coupled scheme offers a trade-off between model accuracy and  
120 computational cost (Yakirevich et al., 1998; Liang et al., 2003), and has been used to  
121 couple two hydrodynamic models with the hydraulic head of the internal boundary  
122 being used as the exchange information (Stoppelenburg et al., 2005; Kuznetsov et al.,  
123 2012). However, the soil water content is the variable used by soil water balance models  
124 other than the hydraulic head. Therefore, a specific iterative scheme should be  
125 developed to couple the soil water balance model using the water content and the  
126 hydrodynamic groundwater model using the hydraulic head.

127 The third concern is about practicability. Many Quasi-3D models are focus on the  
128 algorithms, while lacking the pre- and post-processing tools for handling the spatial  
129 information, which limit the model application for a practical regional scale problem  
130 with complicated hydrogeological properties and boundary conditions (Zhu et al.,  
131 2013).

132 In this study, a new Quasi-3D model is developed. The 1-D water balance model



133 UBMOD developed by Mao et al. (2018) is integrated with MODFLOW (Harbaugh,  
134 2005). A new iterative scheme is established for numerical solutions, and the net  
135 groundwater recharge and **the depth of unsaturated zone** are chosen as the exchange  
136 information. The coupling model can achieve mass balance and keep numerical  
137 stability well, and the model is suitable for large-scale modeling based on the  
138 characteristics of MODFLOW and UBMOD. Moreover, instead of developing a new  
139 package for MODFLOW, a framework of organizing the modeling procedures by  
140 Python scripts is developed, **which wraps the coupled model, pre- and post-processing**  
141 **tools**. The framework embeds a powerful function of geographic information  
142 processing with the help of Python packages for data preparation and results displaying,  
143 thus makes the modeling tool convenient and flexible for practical uses. This paper  
144 elaborates the methodology of coupling the unsaturated and saturated water flow and  
145 the modeling framework in Sect. 2. Two published studies are used to test the  
146 performance of the coupled model when handling different water flow conditions in  
147 Sect. 3. A real-world application to study the regional net groundwater recharge is  
148 presented in Sect. 4.

## 149 **2 Methodology and Model Development**

150 In the new coupled model, the unsaturated-saturated domain is partitioned into a  
151 number of sub-areas in the horizontal direction mainly according to the spatially  
152 distributed inputs (soil types, atmosphere boundary conditions, land uses, and crop  
153 types). A 1-D soil column is used to characterize the average soil water flow in each



154 sub-area, and UBMOD is used to simulate the 1-D soil water flow. MODFLOW is used  
155 to simulate the 3-D groundwater flow of the whole model domain. It assumed that the  
156 flow in the unsaturated zone is in the vertical direction, and that there is only vertical  
157 exchange flux between the unsaturated and saturated zones. It is further assumed that  
158 using the vertical column can reasonably simulate the unsaturated flow in each sub-area  
159 while ignoring the horizontal heterogeneity. In this section, UBMOD is first presented,  
160 followed by a brief introduction of MODFLOW and two peripheral tools (FloPy  
161 (Bakker et al., 2016) and ArcPy (Toms, 2015) used in the new model. The procedures  
162 of the new model and the modeling framework are described in Sect. 2.3 and the  
163 specific unsaturated and saturated coupling scheme is described in Sect. 2.4.

## 164 **2.1 The Soil Water Balance Model UBMOD**

165 This section briefly describes the soil water balance model UBMOD to make this  
166 paper self-contained, and more details of UBMOD are referred to Mao et al. (2018).  
167 Before the calculation, the domain is discretized into a series of soil layers, and the  
168 simulation period is discretized into time steps. UBMOD has four major components  
169 to describe the soil water movement in a given time step. The first one is the allocation  
170 of the infiltration water if there is precipitation or irrigation on ground surface, and the  
171 other three components correspond to the three forces (the gravitational potential,  
172 source/sink term for external forces and the matric potential) driving the soil water  
173 movement. The governing equations of the model are as follows,

$$174 \quad q = \min(M \times (\theta_s - \theta), I - I_d), \quad (1)$$



175 for the amount of allocated infiltration water of a given layer,

$$176 \quad \frac{\partial \theta}{\partial t} = -\frac{\partial K(\theta)}{\partial z}, \quad (2)$$

177 for the advective movement driven by the gravitational potential,

$$178 \quad \frac{\partial \theta}{\partial t} = -W, \quad (3)$$

179 for source/sink terms, and

$$180 \quad \frac{\partial \theta}{\partial t} = \frac{\partial}{\partial z} \left( D(\theta) \frac{\partial \theta}{\partial z} \right), \quad (4)$$

181 for diffusive movement driven by the matric potential. In these equations,  $q$  is the

182 amount of allocated water per unit area of the layer [L];  $M$  is the thickness of each soil

183 layer [L];  $\theta$  is the soil water content [ $L^3L^{-3}$ ];  $\theta_s$  is the saturated soil water content [ $L^3L^{-3}$ ]

184  $^3$ ;  $I$  is the quantity of infiltration water per unit area [L];  $I_d$  is the allocated amount of

185 infiltration water per unit area specified before the calculation [L];  $t$  is the time [T];  $K(\theta)$

186 is the unsaturated hydraulic conductivity [ $LT^{-1}$ ] as a function of soil water content;  $z$  is

187 the elevation in the vertical direction [L];  $W$  is the source/sink term [ $T^{-1}$ ] to account for

188 soil evaporation and root uptake term of crop transpiration;  $D(\theta)$  is the hydraulic

189 diffusivity [ $L^2T^{-1}$ ],  $D(\theta) = K(\theta) \times \frac{\partial h}{\partial \theta}$ , where  $h$  is the pressure head [L].

190 The equations are solved in sequence in the UBMOD. The unsaturated hydraulic

191 conductivity  $K(\theta)$  in Eq. (2) is a function of soil water content  $\theta$ . The relationship

192 between  $K(\theta)$  and  $\theta$  is characterized by empirical formulas for the purpose of

193 simplifying calculation and eliminating the needs of soil hydraulic parameters. These

194 empirical formulas are referred to as drainage functions, and the commonly used ones



195 can be found in Mao et al. (2018). The diffusion equation (Eq. 4) can be discretized  
196 using an implicit finite difference method, and then solved with the chasing method.  
197 **An empirical formula with four parameters** (saturated hydraulic conductivity  $K_s$ ,  
198 saturated water content  $\theta_s$ , field capacity  $\theta_f$ , and residual water content  $\theta_r$ ) is used in  
199 Mao et al. (2018) to describe the hydraulic diffusivity  $D(\theta)$ . These parameters have  
200 physical meanings, and are easy to be obtained for large-scale modeling. **A correction**  
201 **term is introduced** to describe the spatial variability of soils, which makes the model  
202 applicable to heterogeneous situations. Both the upward and downward soil water  
203 movement can be simulated by UBMOD, and mass balance is well maintained by the  
204 model. The model can effectively and efficiently capture the features of soil water  
205 movement with coarse discretization in space and time.

## 206 2.2 The Brief Introduction of MODFLOW and Two Peripheral Tools

207 MODFLOW is a computer program that numerically solves the 3-D groundwater  
208 flow equation for a porous medium using a block-centered finite-difference method  
209 (Harbaugh, 2005). The governing equation solved by MODFLOW is

$$210 \quad \frac{\partial}{\partial x_i} \left( K_{ij} \frac{\partial H}{\partial x_j} \right) + W = S_s \frac{\partial H}{\partial t}, \quad (5)$$

211 where  $i = 1 - 3$  indicates the  $x$ ,  $y$ , and  $z$  directions, respectively;  $K_{ij}$  is the saturated  
212 hydraulic conductivity [ $\text{LT}^{-1}$ ];  $H$  is the hydraulic head [ $\text{L}$ ];  $W$  is a volumetric flux per  
213 unit volume representing sources and/or sinks of water [ $\text{L}^3\text{T}^{-1}$ ];  $S_s$  is the specific storage  
214 of the porous material [ $\text{L}^{-1}$ ]; and  $t$  is the time [ $\text{T}$ ].

215 FloPy and ArcPy are the two peripheral tools used in our model development.



216 FloPy (Bakker et al., 2016) is a Python package for creating, running, and post-  
217 processing MODFLOW-based models. Unlike the commonly graphical user interfaces  
218 (GUIs) method, FloPy facilitates user to write a Python script to construct and post-  
219 process MODFLOW models, and it has been shown as a convenient and powerful tool  
220 by Bakker et al. (2016). Geographic information system (GIS) is a helpful tool for  
221 groundwater modeling by providing geospatial database and results presentation (Xu et  
222 al., 2011; Lachaal et al., 2012). ArcPy is an application program interface (API) of  
223 ArcGIS for Python (Toms, 2015), which provides a useful and productive way to  
224 perform geographic data analysis, data conversion, data management, and map  
225 automation with Python.

### 226 **2.3 The Procedures of the New Model and the Modeling Framework**

227 The schematic procedures of the modeling framework are shown in Fig. 1(a),  
228 which are composed of three major parts, including the pre-processing, the coupled  
229 model, and the post-processing. Two Python scripts are developed to facilitate the pre-  
230 processing and post-processing respectively. The coupling scheme is also realized using  
231 the Python script, while UBMOD and MODFLOW are used as the executable programs.  
232 The structure of the framework makes it flexible and expansible, as each component  
233 can be easily updated or replaced.

234 The preparation of geographic input information of the model shown in Fig. 1(b)  
235 is the major component of pre-processing. The geographic information includes the  
236 domain area, boundary conditions, sub-areas, digital elevation model (DEM), hydraulic



237 conductivity and porosity. The shapefile of the domain area (usually irregular in shape)  
238 is first discretized by regular boundary with both active and inactive cells. The  
239 discretized domain can be joined with the shapefile of boundary condition to generate  
240 the “ibound” array of MODFLOW as shown in Fig. 1(b), which is used to specify which  
241 cells are active, inactive, or fixed head in MODFLOW. The shapefile of sub-areas is  
242 joined with the domain file, represented in subareas array with different number  
243 specified as different sub-areas. The raster files of DEM, hydraulic conductivity and  
244 porosity are further joined, and the values of these variables are listed in the arrays  
245 shown in Fig.1 (b). These procedures are implemented automatically by the help of the  
246 pre-processing tool developed by using ArcPy, FloPy and other Python packages. All  
247 these arrays including the geographic information are used by the coupled model for  
248 numerical simulation. The unsaturated-saturated flow model coupling scheme will be  
249 described in next section. The results presentations are accomplished in post-processing  
250 process by post-processing tool, which contains a series of utilities developed based on  
251 Python packages (NumPy, Pandas, Matplotlib, FloPy and other packages)

## 252 **2.4 Coupling Scheme of UBMOD and MODFLOW**

253 Figure 1(c) demonstrates the sketch map of the specific unsaturated and saturated  
254 coupling scheme. The unsaturated-saturated domain is partitioned into a number of sub-  
255 areas in the horizontal direction mainly according to the spatially distributed inputs  
256 (each sub-area is considered to be homogeneous in horizontal). Soil water flow of each  
257 sub-area is simulated by using one 1-D soil column. The whole saturated zone is



258 discretized into a grid with cells, as shown in Fig. 1(c). All cells in the same sub-area  
259 receive the same recharge from soil zone calculated by the representative 1-D soil  
260 column of the sub-area. While it is feasible to use one soil column for each cell, this is  
261 impractical for most large-scale situations due to unavailable soil data and heavy  
262 computation cost. In the vertical direction, both the saturated domain and the soil  
263 columns are discretized into different layers based on available data and information,  
264 and the layer discretization remain unchanged during the simulation. Note that the  
265 saturated zone and the unsaturated zone are independent, but some layers may  
266 transform between the saturated zone and the unsaturated zone, which are referred as  
267 the **overlap region**. It should ensure that both the discretization and input information  
268 for saturated calculation and unsaturated calculation of the overlap region are assigned.  
269 As shown in the Fig. 1(c), there are  $m$  rows and  $n$  columns cells of the saturated zone,  
270 and  $l$  sub-areas,  $j$  layers for one soil column. The vertical layers for different soil  
271 columns can be different.

272 Since the output variable of UBMOD is the soil water content and the output of  
273 MODFLOW is hydraulic head, this study uses the vertical net recharge and the  
274 unsaturated zone depth to couple the unsaturated zone and saturated zone. **The vertical**  
275 **net recharge is represented by matrix  $\mathbf{R}$  with  $m \times n$  elements**, and the unsaturated zone  
276 depth by vector  **$\mathbf{Du}$**  with  $l$  elements, as illustrated in Fig. 1(c). Scalar  $R$  is used in this  
277 study to denote the specific net recharge of a soil column to the corresponding saturated  
278 sub-area, scalar  $du$  is used to denote the depth of a soil column. A new method is



279 developed to capture the net recharge between unsaturated zone and saturated zone.  
280 Figure 2(a) shows the spatial coupling scheme of a soil column connected with  
281 groundwater system. The water table locates in layer  $j$ . The net recharge  $R$  from  
282 unsaturated zone is calculated via

$$283 \quad R = q_I + q_A - q_S - q_D, \quad (6)$$

284 where  $q_I$  is the flux across the water table caused by allocation of the infiltration water  
285 per unit area [L];  $q_A$  is the flux across the water table caused by the advective movement  
286 per unit area [L];  $q_S$  is the flux across the groundwater table caused by source/sink terms  
287 per unit area [L] and  $q_D$  is the flux across the water table caused by the water diffusion  
288 per unit area [L]. All the  $q$  terms are calculated by UBMOD.

289 Specifically, the infiltration water is allocated first according to the Eq. (1) if there  
290 is precipitation or irrigation. If there is a residual infiltration across the water table in  
291 the  $j$  layer of the unsaturated zone, the amount of residual infiltration is denoted as  $q_I$ .  
292 Then the advective flow  $q_A$  across the water table driven by gravitational potential is  
293 calculated by using Eq. (2). The directions of these two terms are downward. The  $q_S$   
294 term is upward and resulted from groundwater by evapotranspiration. A virtual layer is  
295 needed when calculating the diffusive movement driven by matrix potential across the  
296 water table based on Eq. (4). As shown in Fig.2 (a), the virtual layer will be added under  
297 water table, numbered as layer  $j+1$ . The thickness,  $M_{j+1}$  [L], of the layer is set as,

$$298 \quad M_{j+1} = z_{j+1} - d_u, \quad (7)$$

299 where  $z_{j+1}$  is the bottom depth of layer  $j+1$  [L]. The amount of the upward flux between



300 the virtual layer and layer  $j$  is denoted as  $q_D$ . Then, the net recharge matrix  $\mathbf{R}$  for the  
301 whole area is obtained and used for the Recharge (RCH) package of MODFLOW.

302 The serial coupling scheme is shown in Fig. 2(b). There are three levels of time  
303 discretization in the coupling model (shown in Fig.2(b)) as follows: the stress periods

304  $\Delta T$  used in MODFLOW, the time step  $\Delta t_s$  in each stress period during the saturated

305 calculation, the time steps  $\Delta t_u$  during the unsaturated calculation. The unsaturated zone

306 and saturated zone exchange information at the end of each stress period. Figure 2(c)

307 describes the calculation procedures of the model and the iterative coupling scheme at

308 time  $t$ . The model first reads the inputs of spatial data, prepares the model data and

309 parameters, and updates the data at the beginning of the time or iteration loop. Then the

310 model runs the UBMOD model with the unsaturated time step  $\Delta t_u$  to obtain the vertical

311 recharge. The total recharge during the time level of stress period  $\Delta T$  can be obtained

312 by summarizing the recharge at each time step. The net recharge at time  $t$  and at the  $p$ -

313 th iteration is represented as  $\mathbf{R}_p$ , which used by the MODFLOW RCH package.

314 Subsequently, the model runs the MODFLOW model to obtain the saturated hydraulic

315 head,  $\mathbf{H}_t^p$  ( $m \times n$  dimension), at time  $t$  and at the  $p$ -th iteration. The convergence of the

316 iteration is determined by using the difference of hydraulic head between the present

317  $\mathbf{H}_t^p$  and the previous iteration  $\mathbf{H}_t^{p-1}$ . The convergence criterion is

318 
$$\text{if } \max \left( \left| \mathbf{H}_t^p - \mathbf{H}_t^{p-1} \right| \right) < \varepsilon_H, \quad (8)$$

319 where  $\varepsilon_H$  is a user-specified tolerance [L]. If the criterion is met, the iteration stops, and

320  $\mathbf{H}_t^p$  is the convergent results at time  $t$ , and the model proceeds to the next time step.



321 Otherwise, the iteration continuous to  $p+1$ . The unsaturated depth  $\mathbf{Du}_t^{p+1}$  is updated at  
322 each iteration. Vector  $\mathbf{Hs}_t^p$  ( $l$  dimension) is used to represent the average saturated  
323 hydraulic head over the same sub-area according to  $\mathbf{H}_t^p$ . Then the new unsaturated depth  
324  $\mathbf{Du}_t^{p+1}$  is calculated as follows

$$325 \quad \mathbf{Du}_t^{p+1} = \mathbf{D} - \mathbf{Hs}_t^p, \quad (9)$$

326 where  $\mathbf{D}$  ( $l$  dimension) is the average depth from the soil surface to the bottom in the  
327 same sub-area [L].  $\mathbf{Du}_t^{p+1}$  is set as the input to UBMOD, and the model proceeds to the  
328 next iteration until the convergence creation of Eq. (8) is met.

### 329 **3 Model Evaluation**

330 In this section, two test cases were designed to evaluate the model accuracy and  
331 the performance of the numerical coupling scheme under complicated soil and  
332 boundary conditions. The simulation results were compared with numerical results  
333 obtained using HYDRUS-1D (Šimůnek et al., 2008) and SWMS2D (Šimůnek et al.,  
334 1994), and with published experimental data. For these cases, the mean absolute relative  
335 error ( $ARE$ ) and the root mean squared error ( $RMSE$ ) were used to quantitatively  
336 evaluate the misfit between the simulated results of the developed model and reference  
337 values.  $ARE$  and  $RMSE$  are calculated as,

$$338 \quad ARE = \frac{1}{x} \sum_{i=1}^x \frac{|y_i - Y_i|}{Y_i} \times 100\%, \quad (10)$$

$$339 \quad RMSE = \sqrt{\frac{1}{x} \sum_{i=1}^x (Y_i - y_i)^2}, \quad (11)$$

340 where the subscript  $i$  represents the serial number of the results;  $x$  represents the total



341 number of the results;  $y_i$  is the simulated result of the coupled model and  $Y_i$  is the  
342 reference result.

### 343 3.1 Two Test Cases

#### 344 3.1.1 Case 1: 1D upward flux with atmospheric condition

345 This case was to test the performance of the coupling scheme explained in Sect.  
346 2.4. It considered 1-D water flow in a field profile of the Hupselse Beek watershed in  
347 the Netherlands, which was used as a demo in HYDRUS-1D technical manual  
348 (Šimůnek, 2008). The soil profile consists of a 0.4m-thick upper layer and a 1.9m-thick  
349 bottom layer. The depth of the root zone is 0.3 m. The hydraulic parameters of the two  
350 soil layers are presented in Table 1. The surface boundary condition involves actual  
351 precipitation and potential transpiration rate as shown in Fig. 3. The groundwater level  
352 was initially set at 0.55 m below the soil surface. Only one vertical soil column and one  
353 MODFLOW cell were used in the coupled model. The parameters used in the coupled

354 model are also listed in Table 1. The stress period  $\Delta T$  was set as 5 d, and the  
355 MODFLOW time step  $\Delta t_s$  and the UBMOD time step  $\Delta t_u$  were both set to be 1 d. The  
356 results from HYDRUS-1D were used as the reference of this test case. The mean time  
357 step used in the HYDRUS-1D was 0.13 d. The spatial discretization of UBMOD was  
358 0.1 m, and that of HYDRUS-1D varied between 0.01 m and 0.1 m.

#### 359 3.1.2 Case 2: Two-dimensional (2D) water table recharge experiment

360 This test case was used for model validation in a 2-D unsaturated-saturated flow  
361 system. The numerical simulation of our model was compared with the data of a 2-D



362 water table recharge experiment conducted by Vaulin et al. (1979). The experimental  
363 data have been used to test the variably saturated flow models (Clement et al., 1994)  
364 and coupled unsaturated-saturated flow models (Thoms et al., 2006; Twarakavi et al.,  
365 2008; Shen and Phanikumar, 2010; Xu et al., 2012). The 2-D domain is a rectangular  
366 sandy soil slab of  $6.0 \times 2.0 \times 0.05$  m. The initial pressure head is 0.65 m at the domain  
367 bottom. At the soil surface, a constant flux of  $q = 3.55$  m/d is applied at the central 1.0  
368 m, and the rest soil surface is the no flux boundary. Because of the symmetry of the  
369 flow system, only one half of domain (right side) with the size of  $3.0 \text{ m} \times 2.0 \text{ m} \times 0.05$   
370 was simulated. The setup of the simulation is shown in the Fig. 4(a). No-flow  
371 boundaries were defined on the bottom and the left side, and specified hydraulic head  
372 boundary of 0.65 m was set on the right side. The values of soil hydraulic parameters  
373 are listed in Table 1. The simulation period is 8 h. In our coupled model, there were 30  
374 uniform rectangular cells used by MODFLOW, and there were 10 sub-areas defined to  
375 represent the unsaturated zone, which were numbered from left to right. The first and  
376 last sub-areas covered 0.2 m and 0.4 m in the  $x$  direction respectively, and each the rest  
377 sub-area covered 0.3 m in the  $x$  direction. The first and the second sub-areas were used  
378 to define the recharge boundary, while the others sub-areas were used to define the no-  
379 recharge boundary. The stress period  $\Delta T$  was set as 1 h, and the MODFLOW time step  
380  $\Delta t_s$  and UBMOD time steps  $\Delta t_u$  were set as 0.167 h. The spatial discretization of  
381 UBMOD was uniformly 0.1 m. The experiment was also simulated by using SWMS2D,  
382 which considered the lateral flow. The mean time step of SWMS2D was set to be 0.0225



383 h, and 20, 200 finite elements were used.

## 384 **3.2 Results and Discussions of Model Performance**

### 385 3.2.1 Computational accuracy of the coupling scheme

386 Figure 5 shows the comparison of the results simulated by HYDRUS-1D and the  
387 coupled model of case 1. Figure 5(a) demonstrated that the water table depth calculated  
388 by the coupled model has a similar pattern to that of HYDRUS-1D. The *ARE* and *RMSE*  
389 values were 14.2% and 0.135 m, respectively. The soil water contents at the depth of  
390 1.15m over time from the two models are compared in Fig. 5(b). The *ARE* and *RMSE*  
391 at  $z = 1.15$  m were 1.9% and  $0.008 \text{ cm}^3/\text{cm}^3$ . The simulated soil water content profiles  
392 at different times are shown in Fig. 5(c). The *ARE* and *RMSE* values of different times  
393 were 2.2%, 5.6%, 6.0% and  $0.017 \text{ cm}^3/\text{cm}^3$ ,  $0.017 \text{ cm}^3/\text{cm}^3$ ,  $0.018 \text{ cm}^3/\text{cm}^3$ ,  
394 respectively. These results indicate that the coupled model can capture the flow  
395 information under an upward flux and the heterogeneous condition.

396 Figure 4(b) shows the comparison of simulated water tables at 4 different times  
397 using the coupled model and SWMS2D and the observation data in case 2. The *ARE*  
398 and *RMSE* values are listed in Table 2. The coupled model matched the observation  
399 data well at the simulation times of 3 h, 4 h and 8 h, with the *ARE* values smaller than  
400 3% and the *RMSE* values smaller than 0.03 m. The observed and simulated soil water  
401 content profiles for the initial and ending times are presented in Fig. 6. The *ARE* and  
402 *RMSE* values are also listed in Table 2. The SWMS2D model predicted accurately at  
403 all the locations. The simulations by the coupled model agreed well with the



404 observations at the locations of  $x = 0.2$  m,  $x = 1.4$  m and  $x = 2$  m (Figs. 6(a), (d) and (e))  
405 where the lateral water flow was negligible. These results demonstrated the accuracy  
406 of the coupled model and the reliability of the coupling scheme shown in Sect. 2.4.

### 407 3.2.2 Limitations of the coupled model

408 Although the coupled model had a sufficient computational accuracy as shown  
409 above, there were limitations because of the quasi-3D assumptions. The coupled model  
410 overestimates the water table at the time of 2 h in case 2 as shown in Fig. 4(b). This was  
411 caused by a significant lateral flow in the unsaturated zone during the early period due  
412 to the relatively low initial soil water content condition. Therefore, a portion of the  
413 infiltration water in the first and second sub-areas should move in the lateral direction,  
414 instead of moving downward to the saturated zone as in the Quasi-3D model. The  
415 coupled model thus overestimated the recharge flux, and resulted in a higher water table  
416 at the early period. The *ARE* of groundwater table prediction of coupled model was  
417 11.6% and *RMSE* 0.088m at the simulation time 2 h, which was larger than that of  
418 SWMS2D. Additionally, the simulated soil water content by the coupled model had  
419 poor performance at the locations of  $x = 0.6$  m and  $x = 0.8$  m (Fig. 6(b) and (c)). The  
420 *ARE* values of the coupled model were 80.5% and 52.1% at  $x = 0.6$  m and  $x = 0.8$  m,  
421 which were 11.4% and 21% in the SWMS2D. These two sub-areas were close to the  
422 recharge zone and affected by the lateral flow, which was ignored in the coupled model.  
423 Therefore, the coupled model overestimates the recharge and underestimates the soil  
424 water content when the lateral flow cannot be ignored. Its application should be limited



425 to cases in which the soil flow mainly occurs in the vertical direction.

### 426 3.2.3 Water mass balance and computational cost

427 The mass balance error of the coupled model was small and the maximum value  
428 was 0.0063% in case 1 and 0.0037% in case 2, while it was 1.6% for the HYDRUS-1D  
429 model and 0.133% from the SWMS2D model. The cases were run on a 6 GB RAM,  
430 double 2.93 GHz intel Core (TM) 2 Duo CPU-based personal computer. For case 1, the  
431 simulation time of the coupled model and the HYDRUS-1D model were 81 s and 1.4 s,  
432 respectively. The iteration and information exchange were responsible for the high  
433 computational cost. For case 2, the simulation time of the coupled model and the  
434 SWMS2D model were 46 s and 95 s, respectively. The coupled model had a better  
435 efficiency comparing with the complete 2D model due to its simpler numerical  
436 solutions and coarse discretization in space and time. Therefore, the coupled model  
437 provided satisfactory mass balance and good computational efficiency.

## 438 4 Real-World Application

### 439 4.1 Study Site and Input Data

440 The coupled model was used to calculate the regional-scale groundwater recharge  
441 in a real-world case, where the shallow groundwater has significant impact on the soil  
442 water movement in the study site. Therefore, the widely adopted methods (e.g., such as  
443 INFIL 3.0 developed by Fill (2008)) estimating groundwater recharge without  
444 concerning the groundwater movement may be inadequate for the recharge estimation.  
445 Figure 7(a) shows the location of the study site, the Yonglian irrigation area (107°37'19"



446 - 108°51'04" E, 40°45'57" - 41°17'58" N) in Inner Mongolia, China. The irrigation area  
447 is 12 km long from north to south, and 3 km wide from east to west. The whole domain  
448 size is 29.75 km<sup>2</sup>. The ground surface elevation decreases from 1028.9 m to 1025.4 m  
449 from the southwest to the northeast. A two-year tracer experiment from 2014 to 2016  
450 was conducted to obtain the groundwater recharge (Yang, 2018), and the experimental  
451 locations are shown in Fig. 7(a). This irrigation area has well-defined hydrogeological  
452 borders by the channel network. Since the Zaohuo Trunk Canal and No. 6 Drainage  
453 Ditch are filled with water over the simulation time, the first-kind boundary condition  
454 was applied to the two segments. The non-flow boundary condition was used for the  
455 other segments of the area. The irrigation water of this area is diverted from the Renmin  
456 Canal. This irrigation area was divided into three sub-areas according to the land uses  
457 at the site, which were farm land, villages and bared soil, as shown in Fig. 7(b). The  
458 crop types in the farmland were not considered for determining the sub-areas. The  
459 surface digital elevation model (DEM) is shown in Fig. 7(c).

460 The measured soil water content and groundwater table in the crop growing season  
461 from May to October of 2004 were used to calibrate the hydraulic parameters, and the  
462 tracer experiment from 2014 to 2016 was used for the groundwater recharge evaluation.  
463 A uniform daily rainfall rate was applied to the whole domain. The irrigation water was  
464 only applied to the farm land. The potential evapotranspiration  $ET_0$  in 2004 was  
465 calculated by the measured evaporation data from the 20 cm pan, multiplying by the  
466 conversion coefficient of 0.55 recommended by Hao (2016). The  $ET_0$  during 2014 to



467 2016 was calculated by using the Penman-Monteith equation. The precipitation,  
468 irrigation and  $ET_0$  are shown in Fig. 8. The crop growing season is from May to October,  
469 and the rest months are no-crop growing season. Based on the hydrogeological  
470 characteristics of the study area provided by the Geological Department of Inner  
471 Mongolia, the top aquifer within the depth of 7 m is loamy sand and loam with small  
472 hydraulic conductivity; an underlying sand aquifer with the thickness of 46 m has high  
473 permeability, and the sand aquifer is lying on an impervious 1m-thick clay layer. The  
474 clay layer was used as the bottom of the simulation domain, and seven different  
475 geological layers were used in the MODFLOW model. The first layer was set to be the  
476 top aquifer, and the second aquifer were divided into 6 layers for numerical simulation.  
477 Ten groundwater monitoring wells were set in this district, and the groundwater tables  
478 were observed every 6 days. Well 1, well 2, well 3, well 5 and well 6 are located in the  
479 farm land area, well 4 and well 8 in a village, and well 7, well 9 and well 10 in a bared  
480 soil area. Additionally, there are 5 soil water content monitoring points in the farm land  
481 and 2 points in the bared soil area, as shown in Fig.7(a). Soil water contents within 1 m  
482 depth were observed 1-3 times every month from May to October in 2004.

483 Five GIS files are prepared as the shapefile files of the study domain, the land use  
484 types, the boundary conditions, and raster files of the surface DEM and initial hydraulic  
485 head. There were 150 rows and 50 columns used in the MODFLOW model. The spatial  
486 discretization of UBMOD was set to be 0.1 m. The stress period  $\Delta T$  was set as 5 d, and  
487 the MODFLOW time step  $\Delta t_s$  and UBMOD time step  $\Delta t_u$  were set as 1 d.



#### 488 4.2 Model Calibration Results

489 There were two soil types in the first layer as loamy sand and loam. The  
490 unsaturated hydraulic parameters of the two soils are listed in Table 3. The hydraulic  
491 conductivity of the top aquifer in MODFLOW was set as the same as the unsaturated  
492 layer, the hydraulic conductivity of the bottom sand aquifer was set as 3.5 m/d during  
493 the calibration, and the specific yields of the top and bottom were set as 0.08 and 0.1,  
494 respectively. Figure 9 shows the comparison of the simulated and observed water table  
495 depth for the four areas, i.e., the whole area, farm land, village, and bared soil. The  
496 measured water table depths were averaged according to the land use types. The *ARE*  
497 values of four areas are 17.1%, 20.0%, 21.2%, 23.0%, respectively, and the *RMSE*  
498 values of the four areas are 0.306 m, 0.261 m, 0.421 m, 0.428 m, respectively. Figure  
499 10 further shows the spatial distribution of the simulated water table depth at different  
500 output times. The increase trend is obviously found from Fig. 10(a) to Fig. 10(c) in the  
501 farm land, during which the groundwater was consumed by crop transpiration and soil  
502 evaporation, while slight changes are found in the non-farm land. When the intensive  
503 autumn irrigation happened after the 160<sup>th</sup> day, the water table depth in the farm land  
504 decreased rapidly, as shown in Fig. 10(d). These results indicate that our model can  
505 reasonably simulate the saturated water table depth in space and time.

506 Figure 11 shows the comparison between the simulated and average observed soil  
507 water content profiles of the farm land and bared soil at different times. The *ARE* values  
508 of the farm land at the times of 40d, 85d, 125d, and 166d were 26.2%, 24.4%, 27.5%,



509 29.1%, respectively, and the *RMSE* values of the four times are 0.009 cm<sup>3</sup>/cm<sup>3</sup>, 0.073  
510 cm<sup>3</sup>/cm<sup>3</sup>, 0.083 cm<sup>3</sup>/cm<sup>3</sup>, 0.088 cm<sup>3</sup>/cm<sup>3</sup>, respectively. The corresponding values for the  
511 bared soil were 15.5%, 18.1%, 12.8%, 14.0% and 0.055 cm<sup>3</sup>/cm<sup>3</sup>, 0.055 cm<sup>3</sup>/cm<sup>3</sup>, 0.041  
512 cm<sup>3</sup>/cm<sup>3</sup>, 0.032 cm<sup>3</sup>/cm<sup>3</sup>, respectively. The observations had higher soil water content  
513 in the root zone than those from the simulations in the farm land. The sampling points  
514 located at the border of fields, which leads to an overestimation of the soil water content  
515 in the root zone due to less crop root uptake. The simulated soil water content profiles  
516 in the bared soil agreed well with the observations.

517

#### 518 4.3 Regional Groundwater Recharge

519 In the tracer experiment, bromide (Br) was used as the tracer for calculating  
520 groundwater recharge. The tracer was injected at 1 m depth at two points shown in Fig.  
521 7(a) in October, 2014. Based on two sampling in October of 2015 and 2016, the  
522 downward recharge is estimated according to the movement of the tracer peak. As  
523 shown in Table 4, the annual average recharge *R* was 33.8 mm/year, and the recharge  
524 coefficient was 0.055 during the period of 2014 - 2016.

525 The calibrated coupled model was used to estimate the groundwater recharge from  
526 October 1, 2014 to September 30, 2016. Figure 12 shows the time series of simulated  
527 recharge rate in the farm land, and Table 4 lists the simulation results. The simulation  
528 results indicate that groundwater is recharged in the no-crop growing season and  
529 consumed in the crop growing season. The two peak values of groundwater recharge in



530 Fig. 12 are due to the autumn irrigation after harvest for washing salt out. The no-crop  
531 growing season provided 66.3 mm/year groundwater recharge over a year and the  
532 average recharge coefficient was 0.249, which indicates that the autumn irrigation in  
533 the no-crop growing season provided the primary groundwater recharge in the year. In  
534 the crop growth season, the recharge was negative, which meant that groundwater was  
535 consumed by crop transpiration and soil evaporation. As calculated by the coupled  
536 model, the annual groundwater recharge was 28 mm/year during the period from  
537 October 1, 2014 to September 30, 2016 in the farm land, which was similar to the result  
538 of the tracer experiment. The results confirmed the coupled model for groundwater  
539 recharge evaluation, which was helpful for scheduling the irrigation amount in the crop  
540 growing season under the water saving policies.

541

## 542 **5 Conclusions**

543 This study developed a new Quasi-3D coupled model for the purpose of practical  
544 modeling of unsaturated-saturated flow at the regional scale. The 1-D water balance  
545 model UBMOD describing the unsaturated soil water flow was integrated with  
546 MODFLOW iteratively. A developed framework implemented the modeling  
547 procedures, and provided the pre- and post-processing tools. The model was evaluated  
548 by using both synthetic numerical examples and real-world experimental data. The  
549 major conclusions drawn from this research are as follows,

550 (1) The new iteration coupling scheme iteratively integrating a hydrodynamic model



551 with a water balance model is reliable. The vertical net recharge and the depth of  
552 the unsaturated zone are effective to be used as the exchange information to couple  
553 the unsaturated zone and saturated zone.

554 (2) The satisfactory results in the two testing examples demonstrate the effectiveness  
555 of the new Quasi-3D model with an acceptable calculative efficiency and well  
556 maintained mass balance.

557 (3) The model gives a satisfactory performance for calculating the groundwater  
558 recharge measured from the tracer experiment. The calculated annual groundwater  
559 recharge is 28 mm/year and the recharge coefficient is 0.046 in the study area.

560 (4) The proposed framework makes the model easy to be expanded, and it gives a  
561 complete solution from geographic information preparation to results displaying  
562 simply and conveniently, even for a complex practical problem.

563 (5) The coupled model should not be used for problems with substantial lateral flow in  
564 the unsaturated zone because of the quasi-3D assumptions used in the model.

565

## 566 Acknowledgments

567 The study was supported by Natural Science Foundation of China through Grants  
568 51790532, 51779178, and 51629901. Requests for data not explicitly provided in the  
569 manuscript may be made to the corresponding author.

570

## 571 References



- 572 Bakker, M., Post, V., Langevin, C., Hughes, J., White, J., Starn, J. and Fienen, M.:  
573 Scripting MODFLOW model development using Python and FloPy, *Groundwater*,  
574 54(5), 733-739, doi:10.1111/gwat.12413, 2016.
- 575 Bouwer, H.: Integrated water management: emerging issues and challenges, *Agric.*  
576 *Water Manage.*, 45(3), 217-228, doi:10.1016/S0378-3774(00)00092-5, 2000.
- 577 Brunner, P. and Simmons, C.: HydroGeoSphere: a fully integrated, physically based  
578 hydrological model, *Groundwater*, 50(2), 170-176, doi:10.1111/j.1745-  
579 6584.2011.00882.x, 2012.
- 580 Clement, T., Wise, W. and Molz, F.: A physically based, two-dimensional, finite-  
581 difference algorithm for modeling variably saturated flow, *J. Hydrol.*, 161(1-4),  
582 71-90, doi:10.1016/0022-1694(94)90121-X, 1994.
- 583 Diersch, H.: FEFLOW: finite element modeling of flow, mass and heat transport in  
584 porous and fractured media, Springer Science & Business Media, Berlin, German,  
585 2013.
- 586 Downer, C. and Ogden, F.: Appropriate vertical discretization of Richards' equation for  
587 two-dimensional watershed-scale modelling, *Hydrol. Process.*, 18(1), 1-22,  
588 doi:10.1002/hyp.1306, 2004.
- 589 Evans, R. and Sadler, E.: Methods and technologies to improve efficiency of water use,  
590 *Water Resour. Res.*, 44(7), doi:10.1029/2007WR006200,2008, 2008.
- 591 Facchi, A., Ortuani, B., Maggi, D. and Gandolfi, C.: Coupled SVAT-groundwater  
592 model for water resources simulation in irrigated alluvial plains, *Environ. Modell.*



- 593           Softw., 19(11), 1053-1063, doi:10.1016/j.envsoft.2003.11.008, 2004.
- 594   Ferman, A.: Modeling coupled surface-subsurface flow processes: a review, *Vadose*  
595           *Zone J.*, 7(2), 741-756, doi:10.2136/vzj2007.0065, 2008.
- 596   FILL, V.: Documentation of Computer Program INFIL3.0-A Distributed-Parameter  
597           Watershed Model to Estimate Net Infiltration Below the Root Zone, U.S.  
598           Geological Survey, Virginia, U.S., 2008.
- 599   Graham, D. and Butts, M.: Flexible, integrated watershed modelling with MIKE SHE,  
600           in: *Watershed Models*, edited by: Singh, V., and Frevert, D., CRC Press, Cleveland,  
601           Ohio, U.S., 2005.
- 602   Hao, P.: Regional soil water-salt balance in Hetao Irrigation District with drip irrigation  
603           and combined use of surface water and groundwater, Master thesis, School of  
604           Water Resources and Hydropower Engineering, Wuhan University, China, 24 pp.,  
605           2016.
- 606   Harbaugh, A.: MODFLOW-2005, the U.S. Geological Survey modular ground-water  
607           model -- the Ground-Water Flow Process, U.S. Geological Survey, Virginia, U.S.,  
608           2005.
- 609   Harter, T. and Hopmans, J.: Role of vadose zone flow processes in regional scale  
610           hydrology: Review, opportunities and challenges, In: *Unsaturated Zone Modeling:*  
611           *Progress, Challenges and Applications*, editor by: Feddes, R., de Rooij, G., van  
612           Dam, J., Kluwer Academic Publishers, Dordrecht, Netherlands, 179–210, 2004.
- 613   Havard, P., Prasher, S., Bonnell, R. and Madani, A.: Linkflow, a water flow computer



- 614 model for water table management: Part I. Model development, T. ASABE., 38(2),  
615 481-488, doi:10.13031/2013.27856, 1995.
- 616 Karandish, F., Salari, S. and Darzi-Naftchali, A.: Application of virtual water trade to  
617 evaluate cropping pattern in arid regions, Water Resour. Manage., 29(11), 4061-  
618 4074, doi:10.1007/s11269-015-1045-4, 2015.
- 619 Kim, N., Chung, I., Won, Y. and Arnold, J.: Development and application of the  
620 integrated SWAT–MODFLOW model, J. Hydrol., 356(1-2): 1-16,  
621 doi:10.1016/j.jhydrol.2008.02.024, 2008.
- 622 Kuznetsov, M., Yakirevich, A., Pachepsky, Y., Sorek, S. and Weisbrod, N.: Quasi 3D  
623 modeling of water flow in vadose zone and groundwater, J. Hydrol., 450, 140-149,  
624 doi:10.1016/j.jhydrol.2012.05.025, 2012.
- 625 Lachaal, F., Mlayah, A., Bédir, M., Tarhouni, J. and Leduc, C.: Implementation of a 3-  
626 D groundwater flow model in a semi-arid region using MODFLOW and GIS tools:  
627 The Zéramdine–Béni Hassen Miocene aquifer system (east-central Tunisia),  
628 COMPUT. GEOSCI-UK., 48, 187-198, doi:10.1016/j.cageo.2012.05.007, 2012.
- 629 Leterme, B., Gedeon, M., Laloy, E. and Rogiers, B.: Unsaturated flow modeling with  
630 HYDRUS and UZF: calibration and intercomparison. In: MODFLOW and More  
631 2015, Golden, CO, Integrated GroundWater Modeling Center, 2015.
- 632 Liang, X., Xie, Z. and Huang, M.: A new parameterization for surface and groundwater  
633 interactions and its impact on water budgets with the variable infiltration capacity  
634 (VIC) land surface model, J. Geophys. Res-Atmos., 108(D16),



- 635           doi:10.1029/2002JD003090, 2003.
- 636   Mao, W., Yang, J. Zhu, Y., Ye, M., Liu, Z. and Wu, J.: An efficient soil water balance  
637           model based on hybrid numerical and statistical methods, *J. Hydrol.*, 559, 721-735,  
638           doi:10.1016/j.jhydrol.2018.02.074, 2018.
- 639   Maxwell, R., Putti, M., Meyerhoff, S., Delfs, J., Ferguson, I., Ivanov, V., Kim, J.,  
640           Kolditz, O., Kollet, S. and Kumar, M.: Surface-subsurface model intercomparison:  
641           A first set of benchmark results to diagnose integrated hydrology and feedbacks,  
642           *Water Resour. Res.*, 50(2), 1531-1549, doi: 10.1002/2013WR013725, 2014.
- 643   Markstrom, S., Niswonger, R., Regan, R., Prudic, D. and Barlow, P.: GSFLOW-  
644           Coupled Ground-water and Surface-water FLOW model based on the integration  
645           of the Precipitation-Runoff Modeling System (PRMS) and the Modular Ground-  
646           Water Flow Model (MODFLOW-2005), U.S. Geological Survey, Virginia, U.S.,  
647           2008
- 648   Niswonger, R., Prudic, D. and Regan, R.: Documentation of the Unsaturated-Zone  
649           Flow (UZFI) Package for modeling unsaturated flow between the land surface and  
650           the water table with MODFLOW-2005, U.S. Geological Survey, Virginia, U.S.,  
651           2006
- 652   Ranatunga, K., Nation, E. and Barratt, D.: Review of soil water models and their  
653           applications in Australia, *Environ. Modell. Softw.*, 23(9), 1182-1206,  
654           doi:10.1016/j.envsoft.2008.02.003, 2008.
- 655   Seo, H., Šimůnek, J. and Poeter, E.: Documentation of the hydrus package for



- 656        MODFLOW-2000, the us geological survey modular ground-water model,  
657        IGWMC-International Ground Water Modeling Center, U.S., 2007.
- 658    Shen, C. and Phanikumar, M.: A process-based, distributed hydrologic model based on  
659        a large-scale method for surface-subsurface coupling, *Adv. Water Resour.*, 33(12),  
660        1524-1541, doi:10.1016/j.advwatres.2010.09.002, 2010.
- 661    Sherlock, M., McDonnell, J., Curry, D. and Zumbuhl, A.: Physical controls on septic  
662        leachate movement in the vadose zone at the hillslope scale, Putnam County, New  
663        York, USA, *Hydrol. Preprocess.*, 16(13), 2559-2575, doi:10.1002/hyp.1048, 2002.
- 664    Šimůnek, J., van Genuchten, M. T. and Šejna, M.: HYDRUS: Model use, calibration  
665        and validation, *T. ASABE.*, 55(4), 1261-1274, doi:10.13031/2013.42239, 2012.
- 666    Šimůnek, J., Šejna, M., Saito, H., Sakai, M. and van Genuchten, M. T.: The HYDRUS-  
667        1D Software Package for Simulating the Movement of Water, Heat, and Multiple  
668        Solutes in Variably Saturated Media, Version 4.0, HYDRUS Software Series 3,  
669        Department of Environmental Sciences, University of California Riverside,  
670        Riverside, California, U.S., 2008.
- 671    Šimůnek, J., Vogel, T. and van Genuchten, M. T.: The SWMS\_2D code for simulating  
672        water flow and solute transport in two-dimensional variably saturated media,  
673        Research Report, California, U.S., 1994.
- 674    Sophocleous, M.: Groundwater recharge and sustainability in the High Plains aquifer  
675        in Kansas, USA, *Hydrogeol. J.*, 13(2), 351-365, doi:10.1007/s10040-004-0385-6,  
676        2005.



- 677 Stoppelenburg, F., Kovar, K., Pastoors, M. and Tiktak, A.: Modelling the interactions  
678 between transient saturated and unsaturated groundwater flow, RIVM report  
679 500026001, 2005.
- 680 Szymkiewicz, A., Gumuła-Kawęcka, A., Šimůnek, J., Leterme, B., Beegum, S.,  
681 Jaworska-Szulc, B., Pruszkowska-Caceres, M., Gorczewska-Langner, W.,  
682 Angulo-Jaramillo, R. and Jacques, D.: Simulations of freshwater lens recharge and  
683 salt/freshwater interfaces using the HYDRUS and SWI2 packages for  
684 MODFLOW, *J. Hydrol. Hydromech.*, 66(2), 246-256, doi: 10.2478/johh-2018-  
685 0005, 2018.
- 686 Tan, X., Wu, J., Cai, S. and Yang, J.: Characteristics of groundwater recharge on the  
687 North China Plain. *Groundwater*, 52(5), 798-807, doi:10.1111/gwat.12114, 2014.
- 688 Thoms, R., Johnson, R. and Healy, R.: User's guide to the variably saturated flow (VSF)  
689 process for MODFLOW. U.S. Geological Survey Techniques and Methods 6-A18,  
690 Virginia, U.S., 58 pp., 2006.
- 691 Tian, Y., Zheng, Y., Wu, B., Wu, X., Liu, J. and Zheng, C.: Modeling surface water-  
692 groundwater interaction in arid and semi-arid regions with intensive agriculture,  
693 *Environ. Modell. Softw.*, 63, 170-184, doi:10.1016/j.envsoft.2014.10.011, 2015.
- 694 Toms, S.: *ArcPy and ArcGIS-Geospatial Analysis with Python*, Packt Publishing Ltd,  
695 Birmingham, UK, 2015.
- 696 Twarakavi, N., Šimůnek, J. and Seo, H.: Evaluating interactions between groundwater  
697 and vadose zone using the HYDRUS-based flow package for MODFLOW,



- 698 Vadose Zone J., 7(2), 757-768, doi:10.2136/vzj2007.0082, 2008.
- 699 Van Walsum, P. and Groenendijk, P.: Quasi steady-state simulation of the unsaturated  
700 zone in groundwater modeling of lowland regions, Vadose Zone J., 7(2), 769-781,  
701 doi:10.2136/vzj2007.0146, 2008.
- 702 VanderKwaak, J. and Loague, K.: Hydrologic - response simulations for the R - 5  
703 catchment with a comprehensive physics - based model, Water Resour. Res.,  
704 37(4), 999-1013, doi:10.1029/2000WR900272, 2001.
- 705 Varado, N., Ross, P. and Haverkamp, R.: Assessment of an efficient numerical solution  
706 of the 1D Richards equation on bare soil, J. Hydrol., 323(1-4), 244-257,  
707 doi:10.1016/j.jhydrol.2005.07.052, 2006.
- 708 Vauclin, M., Khanji, J. and Vachaud, G.: Experimental and numerical study of a  
709 transient, two-dimensional unsaturated-saturated water table recharge problem,  
710 Water Resour. Res., 15(5), 1089-1101, doi:10.1029/WR015i005p01089, 1979.
- 711 Wang, W., Zhang, Z., Yeh, T., Qiao, G., Wang, W., Duan, L., Huang, S. and Wen, J.:  
712 Flow dynamics in vadose zones with and without vegetation in an arid region, Adv.  
713 Water Resour., 106, 68-79, doi:10.1016/j.advwatres.2017.03.011, 2017.
- 714 Weill, S., Mouche, E. and Patin, J.: A generalized Richards equation for  
715 surface/subsurface flow modeling, J. Hydrol., 336(1-4), 9-20,  
716 doi:10.1016/j.jhydrol.2008.12.007, 2009.
- 717 Xu, X., Huang, G., Qu, Z. and Pereira, L.: Using MODFLOW and GIS to access  
718 changes in groundwater dynamics in response to water saving measures in



- 719 irrigation districts of the upper Yellow River basin, *Water Resour. Manage.*, 25(8),  
720 2035-2059, doi:10.1007/s11269-011-9793-2, 2011.
- 721 Xu, X., Huang, G., Zhan, H., Qu, Z. and Huang, Q.: Integration of SWAP and  
722 MODFLOW-2000 for modeling groundwater dynamics in shallow water table  
723 areas, *J. Hydrol.*, 412, 170-181, doi:10.1016/j.jhydrol.2011.07.002, 2012.
- 724 Yakirevich, A., Borisov, V. and Sorek, S.: A quasi three-dimensional model for flow  
725 and transport in unsaturated and saturated zones: 1. Implementation of the quasi  
726 two-dimensional case, *Adv. Water Resour.*, 21(8), 679-689, doi:10.1016/S0309-  
727 1708(97)00031-6, 1998.
- 728 Yang, J., Zhu, Y., Zha, Y. and Cai, S.: Mathematical model and numerical method of  
729 groundwater and soil water movement, Science press, Beijing, China, 2016.
- 730 Yang, X.: Soil salt balance in Hetao Irrigation District based on the SaltMod and tracer  
731 experiment, Master thesis, School of Water Resources and Hydropower  
732 Engineering, Wuhan University, China, 44 pp., 2018.
- 733 Zha, Y., Yang, J., Yin, L., Zhang, Y., Zeng, W. and Shi, L.: A modified Picard iteration  
734 scheme for overcoming numerical difficulties of simulating infiltration into dry  
735 soil, *J. Hydrol.* 551, 56-69, doi:10.1016/j.jhydrol.2017.05.053, 2017.
- 736 Zhang, J., Zhu, Y., Zhang, X., Ye, M. and Yang, J.: Developing a long short-term  
737 memory (LSTM) based model for predicting water table depth in agricultural areas,  
738 *J. Hydrol.*, 561, 918-929, doi:10.1016/j.jhydrol.2018.04.065, 2018.
- 739 Zhu, Y., Shi, L., Lin, L., Yang, J. and Ye, M.: A fully coupled numerical modeling for



740 regional unsaturated-saturated water flow, J. Hydrol., 475(12), 188-203,

741 doi:0.1016/j.jhydrol.2012.09.048, 2012.

742 Zhu, Y., Shi, L., Yang, J., Wu, J. and Mao, D.: Coupling methodology and application

743 of a fully integrated model for contaminant transport in the subsurface system, J.

744 Hydrol., 501, 56-72, doi:10.1016/j.jhydrol.2013.07.038, 2013.

745

746



747

## LIST OF TABLES

748 Table 1. The hydraulic parameters of case 1 and case 2.

	Depth (m)	The parameters used by HYDRUS-1D/SWMS2D and the coupled model			The parameters used only by HYDRUS- 1D/SWMS2D		The parameters used only by the coupled model	
		$\theta_r$ (-)	$\theta_s$ (-)	$K_s$ (m/d)	$n$	$\alpha$ (1/m)	$\theta_f$ (-)	$\mu$
Case 1	0-0.4	0.001	0.399	0.2975	1.3757	1.74	0.26	-
	0.4-2.3	0.001	0.339	0.4534	1.6024	1.39	0.22	0.1
Case 2	0-2.0	0.001	0.3	8.4	4.1	3.3	0.15	0.15

749 #  $\theta_r$  is the residual water content ( $L^3L^{-3}$ );  $\theta_s$  is the saturated water content ( $L^3L^{-3}$ );  $K_s$  is the saturated750 hydraulic conductivity ( $LT^{-1}$ );  $\alpha$  ( $L^{-1}$ ) and  $n$  (-) are parameters depending on the pore size distribution;751  $\theta_f$  is the field capacity ( $L^3L^{-3}$ ) and  $\mu$  is the specific yield (-).

752

753

754 Table 2. The *ARE* and *RMSE* values of SWMS2D and coupled model of case 2.

Water table		$t = 2$ h	$t = 3$ h	$t = 4$ h	$t = 8$ h	
<i>ARE</i> (%)	SWMS2D	0.9%	1.5%	1.6%	1.8%	
	Coupled model	11.6%	2.4%	2.9%	1.6%	
<i>RMSE</i> (m)	SWMS2D	0.010	0.014	0.016	0.022	
	Coupled model	0.088	0.025	0.029	0.021	
Soil water content profile		$x=0.2$ m	$x=0.6$ m	$x=0.8$ m	$x=1.4$ m	$x=2$ m
<i>ARE</i> (%)	SWMS2D	5.6%	11.4%	21.0%	17.6%	6.7%
	Coupled model	12.3%	80.5%	52.1%	27.6%	4.1%
<i>RMSE</i> ( $\text{cm}^3/\text{cm}^3$ )	SWMS2D	0.018	0.031	0.044	0.022	0.017
	Coupled model	0.040	0.173	0.109	0.039	0.010

755

756



757 Table 3. The unsaturated hydraulic parameters.

Soil type	Location	$\theta_f$ (-)	$\theta_s$ (-)	$K_s$ (m/d)	$\theta_f$ (-)
Loamy sand	Village, bared soils	0.065	0.41	1.061	0.18
Loam	Farm land	0.078	0.43	0.2496	0.25

758

759



760 Table 4. The recharge sources and results of the tracer experiment.

	Tracer experiment	Coupled model		
		Crop growing season	No-crop growing season	Annual
$P$ (mm/year)	133.55	100	33.55	133.55
$I$ (mm/year)	477.52	244.27	233.25	477.52
$R$ (mm/year)	33.8	66.3	-38.3	28
$R_c$ (-)	0.055	0.249	-	0.046

761 Note:  $P$  is the annual precipitation;  $I$  is the irrigation water;  $R$  is the annual recharge and  $R_c$  is the

762 recharge coefficient,  $R_c = \frac{R}{(P+I)}$ .

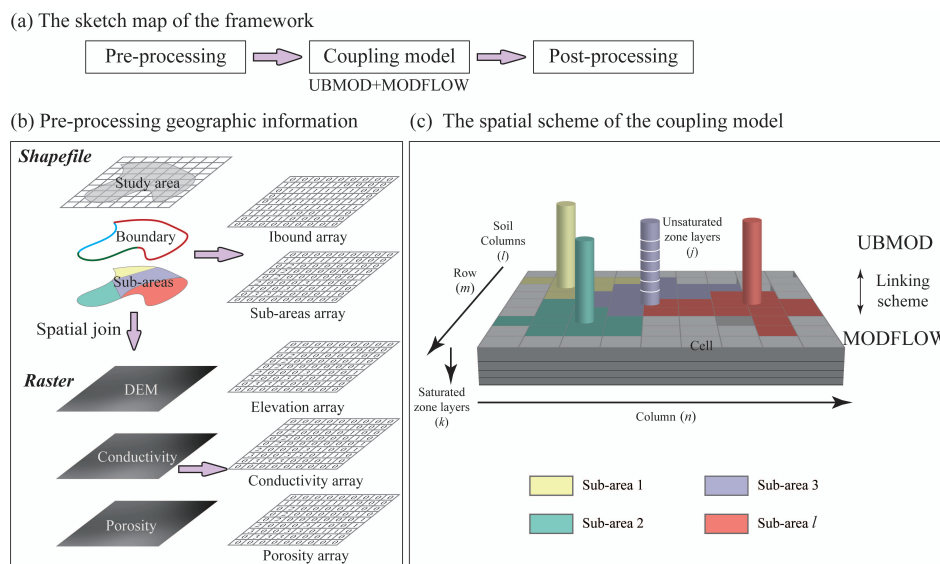
763



764

765

LIST OF FIGURES



766

767

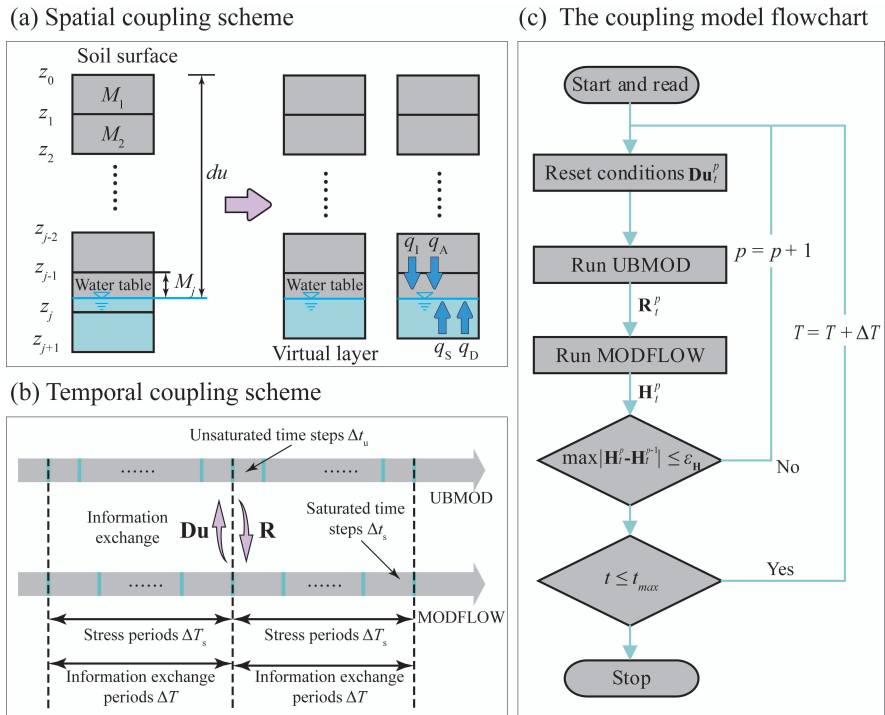
768

769

770

771

Fig. 1. (a) The schematic procedures of the modelling framework. (b) The procedures of geographic input information preparation. (c) The spatial scheme of the coupled model.



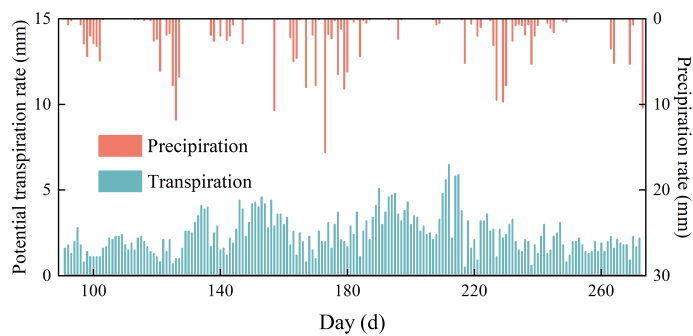
772

773 **Fig. 2.** (a) The spatial coupling scheme. (b) The temporal coupling scheme. (c) The

774 flowchart of the iterative calculation.

775

776

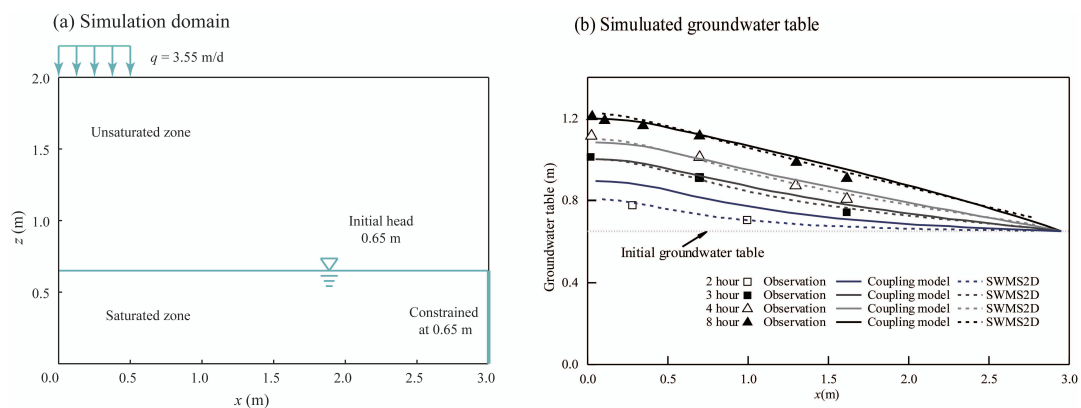


777

778 Fig. 3. The values of actual precipitation and potential transpiration rates.

779

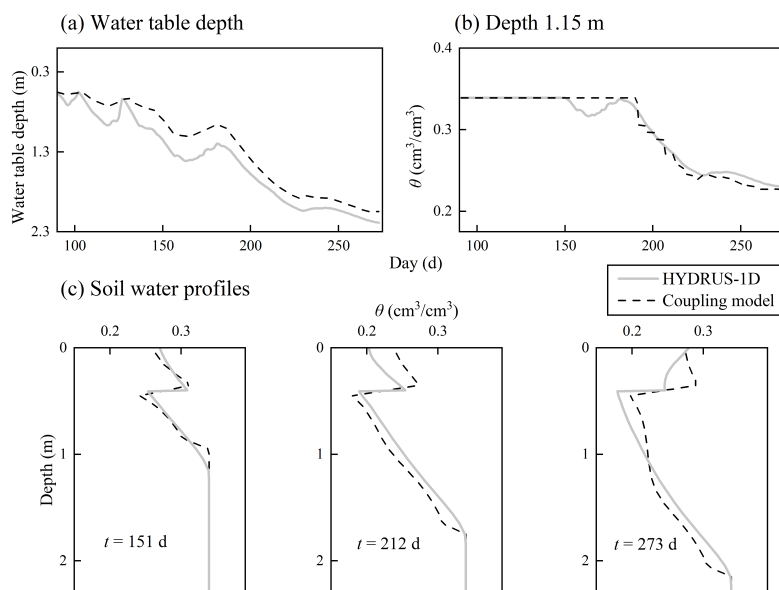
780



781

782 Fig. 4. (a) The sketch of the 2D recharge experiment. (b) The comparison of water table

783 between simulated results by the coupled model, SWMS2D and observation data.



784

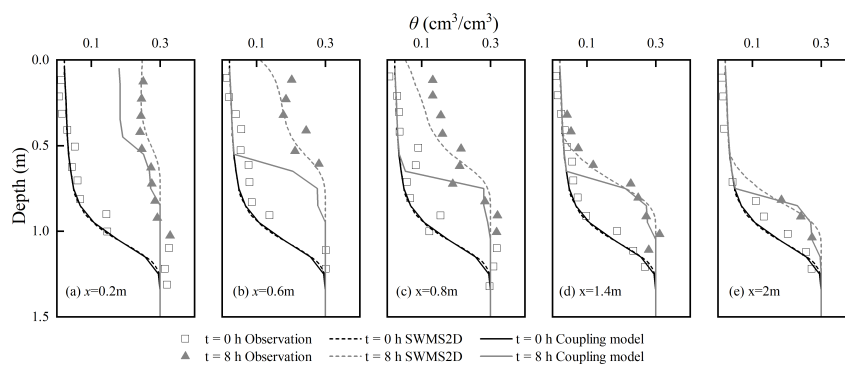
785 Fig. 5. The comparison of the results calculated by HYDRUS-1D and the coupled

786 model in the case 1.

787

788

789



790

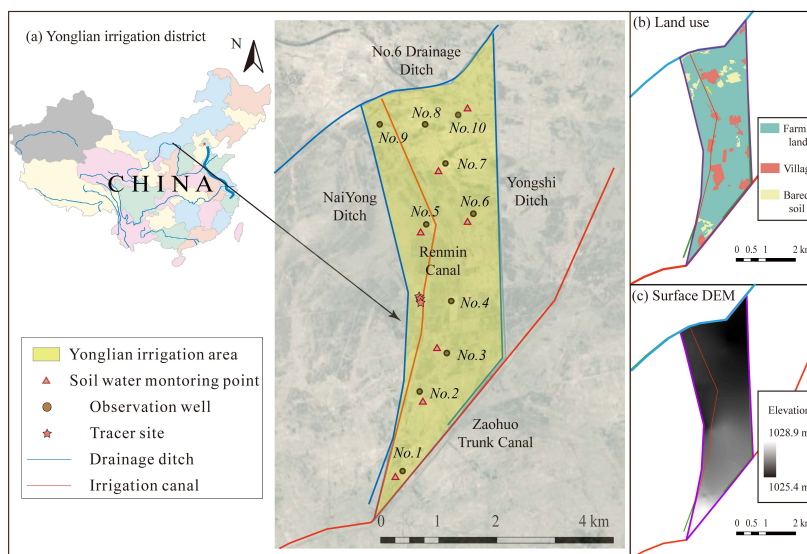
791 Fig. 6. Comparison of soil water content profiles between the simulations from the

792 coupled model, SWMS2D and the observations at different locations: (a)  $x=0.2\text{m}$ ; (b)

793  $x=0.6\text{m}$ ; (c)  $x=0.8\text{m}$ ; (d)  $x=1.4\text{m}$ ; (e)  $x=2\text{m}$ .

794

795



796

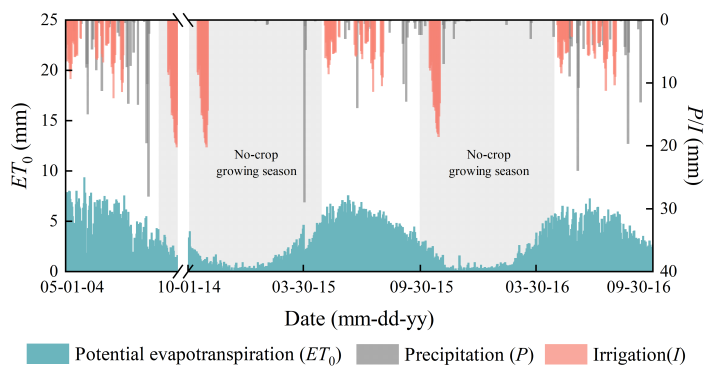
797 Fig. 7. (a) The geographic location Yonglian irrigation area. (b) The land use map. (c)

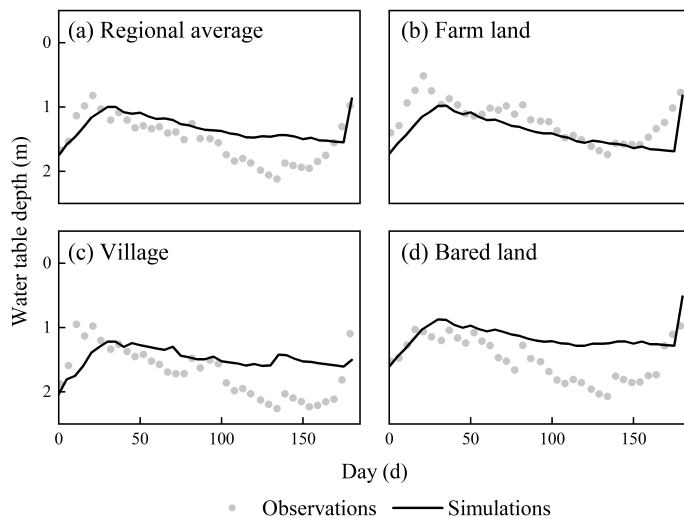
798 The surface DEM.

799

800

801



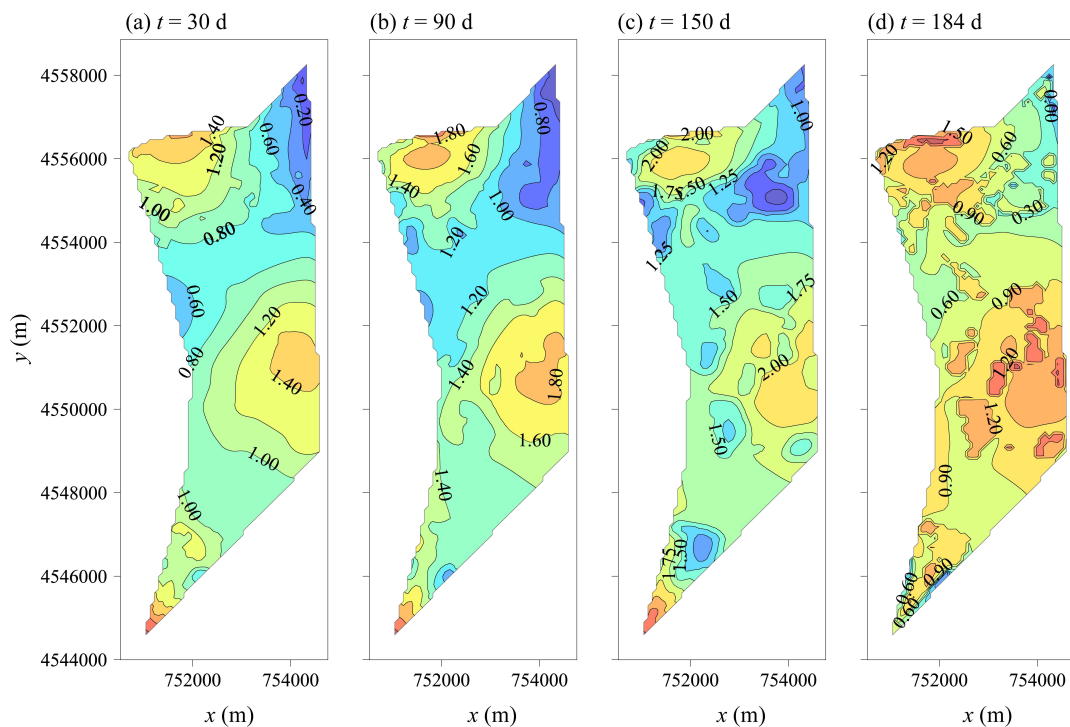


806

807 Fig. 9. Comparison between simulated and observed water table depth.

808

809



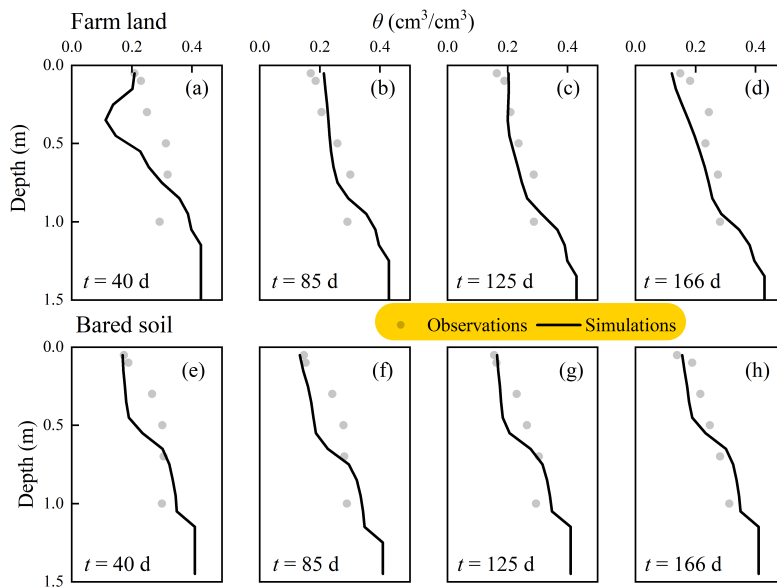
810

811 Fig. 10. Spatial simulated water table depth at different output times.

812

813

814



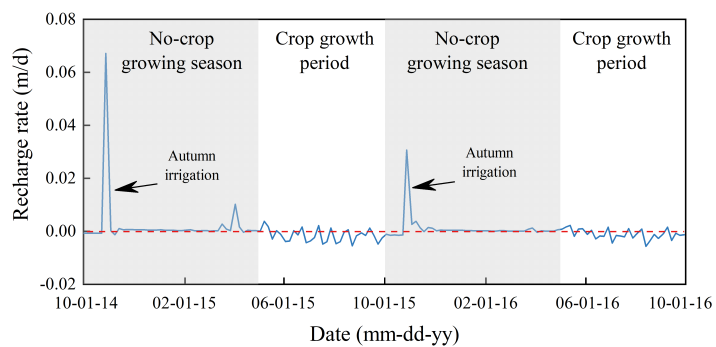
815

816 Fig. 11. Comparison between simulated and observed regional average soil water

817 content profile.

818

819



820

821 Fig. 12. The recharge rate in the farm land calculated by the coupled model

822

823